THE FREQUENCY RESPONSE, COHERENCE, AND INFORMATION CAPACITY OF TWO NEURONAL MODELS

R. B. STEIN, A. S. FRENCH, *and* A. V. HOLDEN

From the Department of Physiology, University of Alberta, Edmonton, Canada. Dr. Holden's present address is the Department of Physiology, University of Leeds, Leeds, England.

ABSTRACT Two neuronal models are analyzed in which subthreshold inputs are integrated either without loss (perfect integrator) or with a decay which follows an exponential time course (leaky integrator). Linear frequency response functions for these models are compared using sinusoids, Poisson-distributed impulses, or gaussian white noise as inputs. The responses of both models show the nonlinear behavior characteristic of a rectifier for sinusoidal inputs of sufficient amplitude. The leaky integrator shows another nonlinearity in which responses become phase locked to cyclic stimuli. Addition of white noise reduces the distortions due to phase locking. Both models also show selective attenuation of high-frequency components with white noise inputs. Input, output, and cross-spectra are computed using inputs having a broad frequency spectrum. Measures of the coherence and information transmission between the input and output of the models are also derived. Steady inputs, which produce a constant "carrier" rate, and intrinsic sources, which produce variability in the discharge of neurons, may either increase or decrease coherence; however, information transmission using inputs with a broad spectrum is generally increased by steady inputs and reduced by intrinsic variability.

I. INTRODUCTION

An increasing number of studies in recent years have attempted to analyze the responses of nerve cells to sensory or synaptic stimuli using systems analysis (see for example the volume edited by Terzuolo [1969]). Other studies have attempted to analyze the statistical pattern of the discharge (Moore et al., 1966) or the ability of nerve cells to convey information (Stein, 1967) using ideas from communications theory (Shannon, 1948). All these results depend both on the properties of the nerve cell as an impulse generator and the properties of the sensory or synaptic inputs used. With a nonlinear system, such as a nerve cell, a relation between stimulus and response as a function of frequency (frequency response function) obtained from a sinusoidal analysis may differ importantly from that obtained with other types of inputs. The differences depend on the type and the magnitude of the nonlinearities.

The use of a random signal with a broad frequency spectrum has considerable advantages (Bendat and Piersol, 1966). The input spectrum, output spectrum, and cross-spectrum can now be obtained conveniently using the fast Fourier transform algorithm (Cooley and Tukey, 1965) both for continuous wave forms and for impulse trains (French and Holden, 1971 *b*). From these spectra the best-fitting frequency response function in the sense of least mean square deviations can be obtained together with the coherence function. The coherence function gives a normalized measure of the extent to which the frequency response function characterizes the properties of the system. The coherence function is also closely related to measures of the information capacity of the system (Stein and French, 1970).

Because of the complexity of nerve cells, it is useful to test these ideas and methods initially on neuronal models which contain some of the essential features of real neurons, but are simpler and can be specified more exactly. One such model which has been used extensively for theoretical studies is a "leaky integrator" in which the effects of brief inputs sum linearly and decay exponentially with a single time constant for voltages up to a threshold (Lapicque, 1907; Stein, 1965; Gluss, 1967; Segundo et al., 1968; Johannesma, 1968; Siebert, 1969; Rescigno et al., 1970; Sugiyama et al., 1970). Beyond threshold an impulse is produced and the voltage of the integrator is quickly reset. We will assume without loss of generality that threshold occurs at a voltage of 1, and that the voltage is immediately reset to 0. If the voltage is reset at time $t = 0$, and the input is $x(t)$, then the voltage $v(t)$ at any time is:

$$v(t) = \int_0^t x(u)\, e^{-(t-u)/\tau}\, du, \tag{1.1}$$

as long as $0 \leq v(t) \leq 1$ for all times between 0 and t.

An important limiting case occurs when $\tau \gg t$. Then:

$$v(t) = \int_0^t x(u)\, du, \tag{1.2}$$

and the model represents a "perfect integrator" for subthreshold voltages. The perfect integrator has been treated as a neuronal model in its own right (Gerstein and Mandelbrot, 1964; Calvin and Stevens, 1968; Bayly, 1968; Knight, 1969; Johannesma, 1969; Knight et al., 1970). The two equations above also occur in the mathematical literature for diffusion processes (Cox and Miller, 1965). If $x(t)$ consists of gaussian white noise, equation 1.1 describes what is known as the Ornstein-Uhlenbeck process, while equation 1.2 is referred to as the Wiener process. The solution for the distribution of times to reach threshold (referred to in the mathematical literature as the first passage time distribution to an absorbing barrier) for equation 1.2 is well known (see, e.g., Gerstein and Mandelbrot, 1964). Although the methods have long been available (Darling and Siegert, 1953), the Laplace transform

of the distribution for equation 1.1 has only recently been obtained (Roy and Smith, 1969; Sugiyama et al., 1970), and the distribution is not available in closed form.

In this paper we will continue to treat the perfect integrator and the leaky integrator separately. Results for the perfect integrator will be considered first, and can largely be derived analytically. Results for the leaky integrator were obtained by simulation where analytic solutions were not possible. Different types of inputs to the two models illustrate different properties, and we have therefore divided the parts of the paper dealing with each model into several sections depending on the type of input used.

II. NOTATION

The following additional quantities will be important in later sections and are listed below together with a brief summary of the methods used to compute them.

$$y(t) = \sum_{i=1}^{k} \delta(t - t_i) \tag{2.1}$$

is the output from the neuronal models, which is treated as a sum of unit impulses (Dirac delta functions) occurring at the times t_i, $1 \leq i \leq k$. Reasons for treating a train of nerve impulses as a sum of unit impulses occurring at points in time (point process), and hence ignoring the shape of the action potential, have been reviewed elsewhere (Stein, 1970). If the duration of the nerve impulse is short compared with the average interspike interval, the spectrum of the response up to frequencies well above the inverse of the average interval will not be affected by the form of the action potential (Nelsen, 1964).

$$X(f) = \int_{-\infty}^{+\infty} x(t)\, e^{-j2\pi ft}\, dt \tag{2.2}$$

is the Fourier integral transform of the input $x(t)$ for a frequency f in Hertz, and $j = \sqrt{-1}$. For computation, $x(t)$ was sampled at 512 equally spaced times. The Fourier integral was replaced by a sum and 256 complex Fourier coefficients were obtained by applying the fast Fourier transform algorithm (Cooley and Tukey, 1965). Details of the methods, developed for the Digital Equipment Corp. PDP-8 computer (Digital Equipment Corp., Maynard, Mass.) which was used in this study, are described elsewhere (French and Holden, 1971 *a*).

$$Y(f) = \int_{-\infty}^{+\infty} y(t)\, e^{-j2\pi ft}\, dt \tag{2.3}$$

is the Fourier integral transform of the output $y(t)$ for a frequency f. $Y(f)$ presents a more formidable computational problem than $X(f)$ since the unit impulses are infinitely brief and hence contain frequency components up to arbitrarily high fre-

quencies. High-frequency components can be confused with low-frequency components (a phenomenon known as *aliasing*) when regular time samples are taken. Our method for overcoming these difficulties has been described in detail elsewhere (French and Holden, 1971 *b*). It consists essentially of convolving each impulse with a $(\sin \theta)/\theta$ function where θ is chosen so that it has no effect on frequencies of interest and completely eliminates all higher frequency components. Such an "ideal" digital low-pass filter can be implemented virtually "on-line" even with a small computer.

$$S_x(f) = X(f)X^*(f) \tag{2.4}$$

is the spectral component of the input signal at frequency f. $X(f)$ will normally be a complex quantity, but the spectrum obtained by multiplying $X(f)$ by its complex conjugate $X^*(f)$ will be real. The spectral component was divided by the difference between the frequencies of successive components Δf to get the *input spectral density* in (volts)^2 per Hertz. The power that is measured physically after filtering is the sum of the components at f and $-f$ and is therefore twice the magnitude given by equation 2.4. Accurate estimates of the spectral density were obtained, often by averaging estimates from 100 samples. For analytical work, it is often more convenient to use the angular frequency, $\omega = 2\pi f$. Then $S_x(\omega) = S_x(f)/2\pi$.

$$S_y(f) = Y(f)Y^*(f) \tag{2.5}$$

is the spectral component of the output signal at frequency f. Normally we computed an *output spectral density* in units of (impulses per second)^2 per Hertz = (impulses)^2 per second.

$$S_{xy}(f) = X(f)Y^*(f) \tag{2.6}$$

gives the cross-spectral component at frequency f. Computed *cross-spectral densities* had units of volts (impulses per second) per Hertz = volts impulses. The cross-spectrum is a complex quantity, containing information about the amplitude and phase of the response as a function of frequency.

$$G(f) = S_{xy}(f)/S_x(f) \tag{2.7}$$

gives the best-fitting *frequency response function* in the sense of least mean square deviation (Bendat and Piersol, 1966). This is also a complex quantity whose magnitude $| G(f) |$ gives the gain and whose argument, $< G(f)$, gives the phase shift of the output with respect to the input.

$$\gamma^2(f) = \frac{| S_{xy}(f) |^2}{S_x(f)S_y(f)} \tag{2.8}$$

is the *coherence function*, and has values such that $0 \leq \gamma^2(f) \leq 1$. The coherence

function will be 1 if the frequency response function completely characterizes the system at the frequency f. The coherence will generally be reduced by any nonlinearities and intrinsic variability in the system and inputs other than $x(t)$ which may impinge on the system. Since $G(f)$ and $\gamma^2(f)$ are ratios, their magnitude will not be affected if $\omega = 2\pi f$ is substituted for f.

III. PERFECT INTEGRATOR

Sinusoidal Inputs

If a sinusoidal modulation of amplitude α is added to a constant input of amplitude c, the input can be written:

$$x(t) = ae^{j(\omega t+\phi)} + c, \tag{3.1}$$

where a wave of angular frequency ω and phase ϕ at time $t = 0$ has been expressed in complex notation. We will only treat real inputs, and will assume implicitly, according to the usual convention, that only the real part of the complex quantity is being considered. Then the input will in fact be a cosine function since $e^{j\phi} = \cos\phi + j\sin\phi$. Substituting equation 3.1 into equation 1.2 and integrating gives the voltage now as a function of ϕ as well as t.

$$v(t, \phi) = \frac{a}{j\omega} e^{j\phi}(e^{j\omega t} - 1) + ct. \tag{3.2}$$

An impulse is generated when the real part of the right-hand side of this equation reaches 1 and the voltage is immediately reset to 0. The value of c determines the rate of impulse generation in the absence of modulation, also referred to as the *carrier rate*. For numerical work, we have set $c = 1$ to give a carrier rate of 1 impulse/sec. If $a \leq c$ it can be shown (Knight, 1969; Rescigno et al., 1970) that as the process continues, impulses are generated at all phases of the input and that the expected density of impulses $h(\phi)$ averaged over a number of cycles is:

$$h(\phi) = ae^{j\phi} + c. \tag{3.3}$$

A proof of this result is included in the section on sinusoidal inputs to a leaky integrator. Equation 3.3 states that for the perfect integrator model (and it holds for this model alone), the density of impulses at various phases of an applied sinusoid will be sinusoidally modulated *with no change in phase and a constant gain at all frequencies.* The modulation of the intervals between impulses, however, (or the instantaneous rate obtained by measuring $1/t_1$ where t_1 is the duration of a single interval) will show distortions in gain and phase (Partridge, 1966; Knight, 1969; McKean et al., 1970). The pattern of impulses will also contain spectral components at multiples of the applied frequency (harmonics) and at many other frequencies (Bayly, 1968).

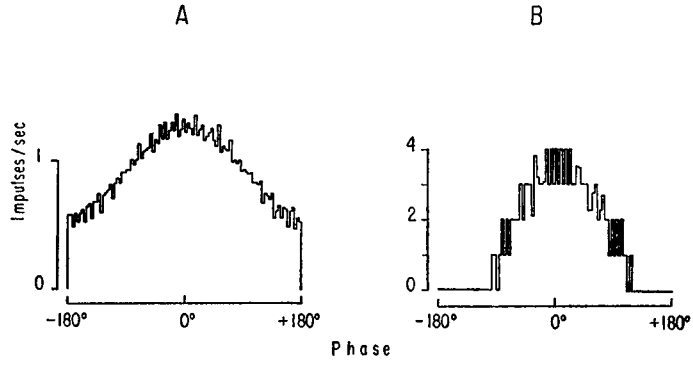

FIGURE 1 Estimates for the impulse density obtained from cycle histograms of a neuronal model operating as a perfect integrator. The model had a carrier rate of 1 impulse/sec which was modulated by a cosine input with a frequency of 0.01 Hz. A shows 40% modulation, while B shows 145% modulation with concomitant rectification of the histogram.

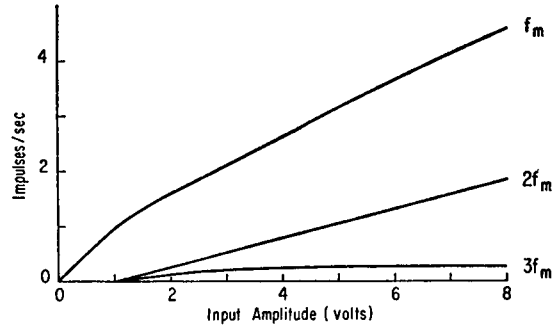

FIGURE 2 Amplitude of the fundamental, the second, and the third harmonics in response to cosine functions of increasing amplitude with a modulating frequency f_m of 0.01 Hz. Up to an input amplitude of 1 v (100% modulation) there is no harmonic distortion and the amplitude of the fundamental f_m increases linearly with the input amplitude; above 100% modulation the amplitude of the fundamental increases asymptotically with half its initial slope, while the amplitude of the second harmonic $2f_m$ increases linearly with increasing input amplitude.

Measured impulse densities are shown in Fig. 1 using an electronic neural analogue (French and Stein, 1970) adjusted to approximate a perfect integrator. In Fig. 1 A, the density follows the applied cosine function, and the reasons for the deviations when the modulation exceeds unity are evident. The impulse density cannot become negative, so it has the appearance of a rectified cosine wave. Harmonics of the applied frequency are present and these grow with increasing modulation until the pattern characteristic of a half-wave rectifier is reached (Fig. 2). Impulse densities showing rectification with sinusoidal inputs have been observed for several types of sensory neurons (e.g. cochlear neurons, Kiang et al., 1965; muscle spindle afferents, Matthews and Stein, 1969; vestibular neurons, Melvill Jones and

Milsum, 1970; cockroach mechanoreceptors, Pearson and Holden, 1970; retinal ganglion cells, Spekreijse and Oosting, 1970).

The effect of one sinusoidally modulated perfect integrator on another is also of interest for the study of synaptic transmission. If r impulses from the first are required to reach threshold and generate one impulse in the second, the impulse density of the impulse train from the second perfect integrator will be simply:

$$h(\phi) = (ae^{j\phi} + c)/r. \tag{3.4}$$

Thus, the ratio of the impulse density of the output train to that of the input train as a function of frequency (frequency response function) for this example is simply:

$$G(\omega) = 1/r, \tag{3.5}$$

independent of ω. This result can easily be extended to any combination of sine or cosine functions and hence to any periodic function of time. If the synaptic effects are purely excitatory, there will be no extra rectification introduced by the second unit. The range of linearity with constant gain and no phase shift would then be infinite! The spectral characteristics of the impulse trains generated by this model will also be derived below.

Poisson Inputs

Let us consider the response of a perfect integrator receiving its input from a source which is generating a purely random or Poisson process with mean rate p. We will again assume that a number r impulses are required to reach threshold and generate one output impulse. A Poisson process is convenient since it contains equal components at all frequencies. The spectral density of the input $S_x(\omega)$ is then simply (Cox and Miller, 1965):

$$S_x(\omega) = p/(2\pi). \tag{3.6}$$

The probability density function $f(t)$ of intervals between output impulses will follow a gamma density function of order r (Cox and Miller, 1965) given by:

$$f(t) = p^r t^{r-1} e^{-pt}/(r-1)! \tag{3.7}$$

This well-known probability density function has a mean $\mu = r/p$, a variance $\sigma^2 = r/p^2$, and a Laplace transform:

$$F(s) \equiv \int_0^\infty f(t)\, e^{-st}\, dt = p^r/(p+s)^r. \tag{3.8}$$

The spectrum of the output pulse train $S_y(\omega)$ can be computed directly from the

Laplace transform of the probability density function (Cox and Miller, 1965) if, as is true here, successive intervals are uncorrelated (renewal process). The spectrum in the presence of a sinusoidally modulated Poisson input has also been computed for $r = 1$ (Knox, 1969). Cox and Miller's formula (p. 359) is in our notation:

$$S_y(\omega) = \frac{1}{2\pi\mu}\left[1 + \frac{F(j\omega)}{1 - F(j\omega)} + \frac{F(-j\omega)}{1 - F(-j\omega)}\right]. \tag{3.9}$$

Substituting equation 3.8 and simplifying:

$$S_y(\omega) = \frac{p}{2\pi r}\frac{(1 + (\omega/p)^2)^r - 1}{[(1 + j\omega/p)^r - 1][(1 - j\omega/p)^r - 1]}. \tag{3.10}$$

The cross-spectrum can easily be obtained from equation 2.7 after substitution from equations 3.5 and 3.6. Then:

$$S_{xy}(\omega) = G(\omega)S_x(\omega) = p/(2\pi r). \tag{3.11}$$

From the spectra of equations 3.6, 3.10, and 3.11, the coherence function defined by equation 2.8 can also be computed:

$$\gamma^2(\omega) = \frac{[(1 + j\omega/p)^r - 1][(1 - j\omega/p)^r - 1]}{r[(1 + (\omega/p)^2)^r - 1]}. \tag{3.12}$$

The limits of this equation are simply:

$$\gamma^2(\omega) = 1, \quad \omega \ll p. \tag{3.13}$$

$$= 1/r, \ \omega \gg p. \tag{3.14}$$

(To obtain the first expression above, expand the factors raised to the rth power, keeping all terms up to $(\omega/p)^2$, and let $\omega/p \to 0$.)

The form of the input spectrum, output spectrum, cross-spectrum, and coherence function are shown in Fig. 3 for $r = 10$ and $r = 3$. Although the input and output are completely coherent at low frequencies, this is not true at high frequencies. The coherence is always less with the larger value of r, and the greatest difference occurs near the carrier rate (1 Hz).

White Noise Inputs

For comparison with the results for a Poisson input, consider a random, continuous input. For simplicity, we assume that all frequency components are equally represented (gaussian white noise), and that the spectral density is:

$$S_x(\omega) = a^2/(2\pi). \tag{3.15}$$

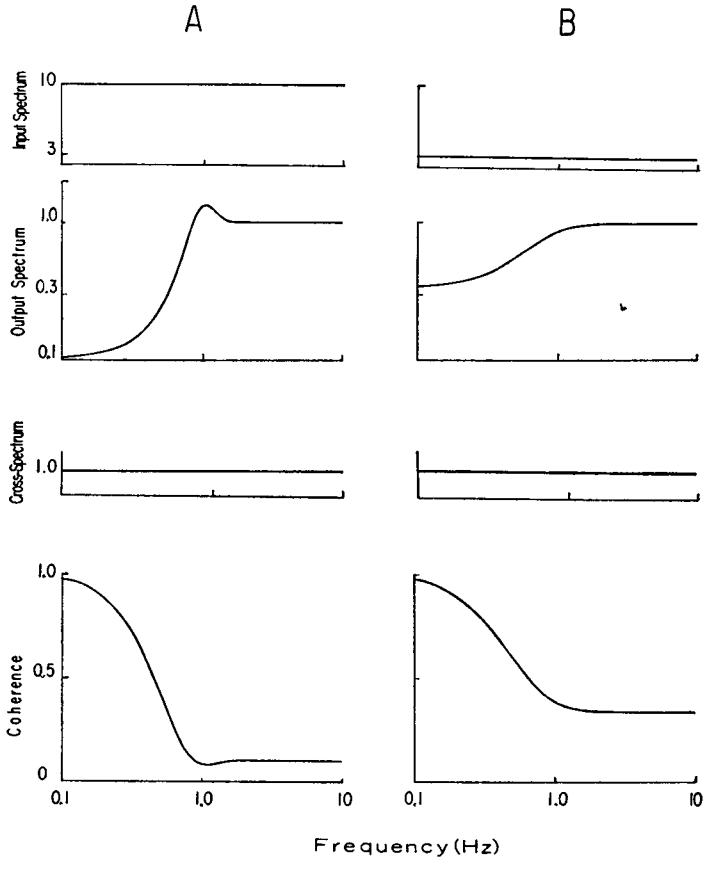

FIGURE 3 The input spectrum, output spectrum, magnitude of the cross-spectrum, and coherence function for a Poisson process applied to the perfect integrator. Definitions and units for these quantities are given under Notation. The values were calculated from equations 3.6, 3.10, 3.11, and 3.12, respectively, assuming (A) $p = r = 10$, or (B) $p = r = 3$. Thus the mean rate was then the same (1 impulse/sec) in A and B, but each output in B required the occurrence of fewer inputs.

It can easily be shown that the root mean square fluctuations in the voltage of the perfect integrator will then be a. These fluctuations may be superimposed upon a constant input c which produces a steady drift in voltage and we have used the same notations as in the previous section on sinusoidal inputs for easy comparison. We assume again that the threshold level is at a voltage of 1, and that upon reaching threshold, the voltage is reset immediately to 0. The interval distribution for this model is well known (see, e.g., Gerstein and Mandelbrot, 1964), and its Laplace transform is in our notation (Sugiyama et al., 1970):

$$F(s) = e^{c/a^2} \exp\left[-(c^2 + 2sa^2)^{1/2}/a^2\right].$$

From the Laplace transform it is easy to show that the mean interval will be $\mu = 1/c$ independent of the level of noise, and the variance will be $\sigma^2 = a^2/c^3$. If we consider a frequency ω, $F(j\omega)$ will be of the form:

$$F(j\omega) = e^{-\alpha}e^{-j\beta}, \tag{3.16}$$

where

$$\alpha = \frac{c}{a^2}(k\cos\theta - 1),$$

$$\beta = \frac{c}{a^2}(k\sin\theta),$$

$$k = [1 + (2\omega)^2(a/c)^4]^{1/4}, \quad \text{and}$$

$$\theta = \tfrac{1}{2}\tan^{-1}[2\omega(a/c)^2].$$

Equation 3.16 can be substituted into equation 3.9 to give the output spectrum.

$$\begin{aligned} S_y(\omega) &= \frac{c}{2\pi}\left[1 + \frac{1}{e^{\alpha+j\beta} - 1} + \frac{1}{e^{\alpha-j\beta} - 1}\right] \\ &= \frac{c}{2\pi}\left[\frac{e^{2\alpha} - 1}{e^{2\alpha} - 2e^{\alpha}\cos\beta + 1}\right]. \end{aligned} \tag{3.17}$$

Note that $S_y(\omega)$ will always be real, even though $F(j\omega)$ is a complex number. This rather formidable-looking expression has simple limits. For small values of ω, we can expand keeping terms up to ω^2.

$$k \backsim 1 + \omega^2(a/c)^4; \qquad \theta \backsim \omega(a/c)^2;$$

$$\alpha \backsim \omega^2a^2/(2c^3); \qquad \beta \backsim \omega/c.$$

and after simplifying:

$$S_y(\omega) = a^2/2\pi. \tag{3.18}$$

Similarly, for large values of ω:

$$k \backsim \sqrt{2\omega}\, a/c; \theta \backsim \pi/4; \alpha \backsim \beta \backsim \sqrt{\omega/a},$$

so that

$$S_y(\omega) = c/(2\pi). \tag{3.19}$$

Limits of the cross-spectrum for this model can also be derived from the form of

the cross-correlation function. Using the definition of the cross-correlation as a time average (Bendat and Piersol, 1966) and equation 2.1, it follows that:

$$C_{xy}(u) = \lim_{T\to\infty} \frac{1}{T} \int_0^T x(t)y(t+u)\,\mathrm{d}t = \lim_{T\to\infty} \frac{1}{T} \sum_{i=1}^{k} x(t_i - u)$$
$$= \nu E\{(t-u)\}, \tag{3.20}$$

where $E\{x(t-u)\}$ is the expected value of $x(t)$ a time u *before* an impulse, and $\nu = k/T$ is the mean rate of nerve impulses.

To determine the expected value of the input at times before or after an impulse, consider a model identical with the perfect integrator except that the voltage on the integrator increases without resetting. Impulses are produced whenever $v(t)$ reaches the next higher integer value. This model will generate impulses at exactly the same times as the perfect integrator, but is mathematically simpler. Equation 1.2 will now hold for all values of v and t, as will the relation:

$$\mathrm{d}v(t)/\mathrm{d}t = x(t).$$

Thus,

$$E\{x(t)\} = \mathrm{d}E\{v(t)\}/\mathrm{d}t. \tag{3.21}$$

We can arbitrarily set $t = 0$ the first time the voltage in this modified process reaches 0 v. The voltage $v(t)$ a time t after the occurrence of this impulse is well known from the theory of diffusion processes. It has a gaussian density function (Johannesma, 1969) which in our notation equals:

$$g(v,t) = \frac{1}{a\sqrt{2\pi t}} \exp\left[\frac{-(v-ct)^2}{2a^2 t}\right].$$

The expected value for $v(t)$ is also known and is just

$$E\{v(t)\} = ct,$$

so

$$E\{x(t)\} = c. \tag{3.22}$$

Thus, for $t > 0$, the cross-correlation function is simply the constant c. For times $t < 0$, the voltages are restricted to values of $v < 0$ and we must consider the first passage time for some value v to 0 in the interval between t and 0. The first passage time from v to 0 in this interval, which has a duration $-t$, is (Johannesma, 1969)

$$f(-t) = \frac{-v}{a\sqrt{2\pi(-t)^3}} \exp\left[\frac{(v-ct)^2}{2a^2 t}\right].$$

Note that $t < 0$, so $-t$ is a positive number and $\sqrt{-t}$ is real. To obtain the expected value the expression above must be multiplied by v, integrated over all permitted values of v, and normalized so that the total probability is unity. Thus,

$$E\{v(t)\} = \frac{\int_{-\infty}^{0} v^2 \exp\left[\frac{(v-ct)^2}{2a^2t}\right] dv}{\int_{-\infty}^{0} v \exp\left[\frac{(v-ct)^2}{2a^2t}\right]}.$$

Let $z = -v/(a\sqrt{-2t})$; then,

$$E\{v(t)\} = \frac{-a\sqrt{-2t}\int_0^{\infty} z^2 \exp\left[-\left(z - \frac{c}{a}\sqrt{\frac{-t}{z}}\right)^2\right] dz}{\int_0^{\infty} z \exp\left[-\left(z - \frac{c}{a}\sqrt{\frac{-t}{z}}\right)^2\right] dz}. \quad (3.23)$$

For sufficiently small values of t

$$E\{v(t)\} = -\alpha\sqrt{-\pi t/2},$$

and

$$E\{x(t)\} = \sqrt{-\pi a^2/(8t)}. \quad (3.24)$$

For large negative values of t, it is easily shown by substituting $z' = z - (c/a)\sqrt{-t/z}$ that the expected value of $x(t)$ is again given by equation 3.22. The constant c will contribute a DC component to the cross-spectrum, whereas the behavior at small values of time will determine the high-frequency part of the cross-spectrum. This can be obtained by substituting equation 3.24 into equation 3.20 and transforming, since the cross-correlation function and the cross-spectrum are a Fourier transform pair (Bendat and Piersol, 1966).

For large ω,

$$S_{xy}(\omega) = \frac{ac}{4\sqrt{2j\omega}}. \quad (3.25)$$

Johannesma (1969, p. 74) showed that the impulse density would follow the input exactly, except for a scaling factor which is equal to unity here. This would suggest that the frequency response function should be equal to unity and the cross-spectrum should be equal to the input spectrum, i.e.,

$$S_{xy}(\omega) = a^2/(2\pi). \quad (3.26)$$

In fact, equation 3.26 is only valid for frequencies below a limiting frequency whose value varies inversely with the amplitude of noise applied. A qualitative

explanation is that the presence of a broad-band input will produce a variability or jitter in the response which will be more deleterious to the transmission of signals the shorter the time period (or the higher the frequency component) considered. Quantitatively, equation 3.25 predicts that the amplitude of the cross-spectrum (and the frequency response function) will decline inversely as the square root of frequency. Phase lags of up to 45° are also introduced.

The limits of the coherence function can be calculated for small values of ω by substituting equations 3.15, 3.18, and 3.26 into the definition for the coherence function (equation 2.8). As for the Poisson process, the various factors cancel, and

$$\gamma^2(\omega) = 1. \tag{3.27}$$

For large values of ω, the coherence function can be obtained using equations 3.15, 3.19, and 3.25. Then,

$$\gamma^2(\omega) = \pi^2 c/(8\omega). \tag{3.28}$$

The coherence depends on the carrier rate c and frequency ω at high frequencies' but it is independent of the input amplitude.

The spectra and coherence for this model when white noise is applied are shown in Fig. 4 choosing values which give the same mean and standard deviation for the interval distribution as those used for the Poisson process in Fig. 3. Then, the output spectrum will be identical with that for the Poisson input at the two extremes of frequency. It is also very similar at intermediate frequencies with the lower level of noise; however, with the higher level of noise, the output spectrum still shows a peak near 1 Hz. In contrast, using a Poisson input, the peak disappears, as the value of r is reduced to 3. The spectrum is then a monotonically increasing function until r is further reduced to 1, where the spectrum becomes flat.

The effects of varying the constant input c while keeping the noise level a constant can also be deduced from the above analysis. First, increasing c will increase the coherence at high frequencies (equation 3.28), while leaving the coherence unchanged at low frequencies. Secondly, the constant c determines the rate at which the integrator charges up, and is also numerically equal to the mean rate at which impulses are discharged. This can be thought of as a carrier rate which is being modulated by the noisy input. Distortion occurs when the modulation ratio (a/c) gets too large (Fig. 1 B) so increasing c will decrease the amount of distortion. Finally, the input and output are completely coherent (i.e., equation 3.27 applies) for a range of frequencies which increases with the value of c. These beneficial effects of increasing the constant input c contrast sharply with the results obtained by introducing some intrinsic variability into the perfect integrator.

Intrinsic Variability

Statistical behavior was present in the input to the model considered above, but the

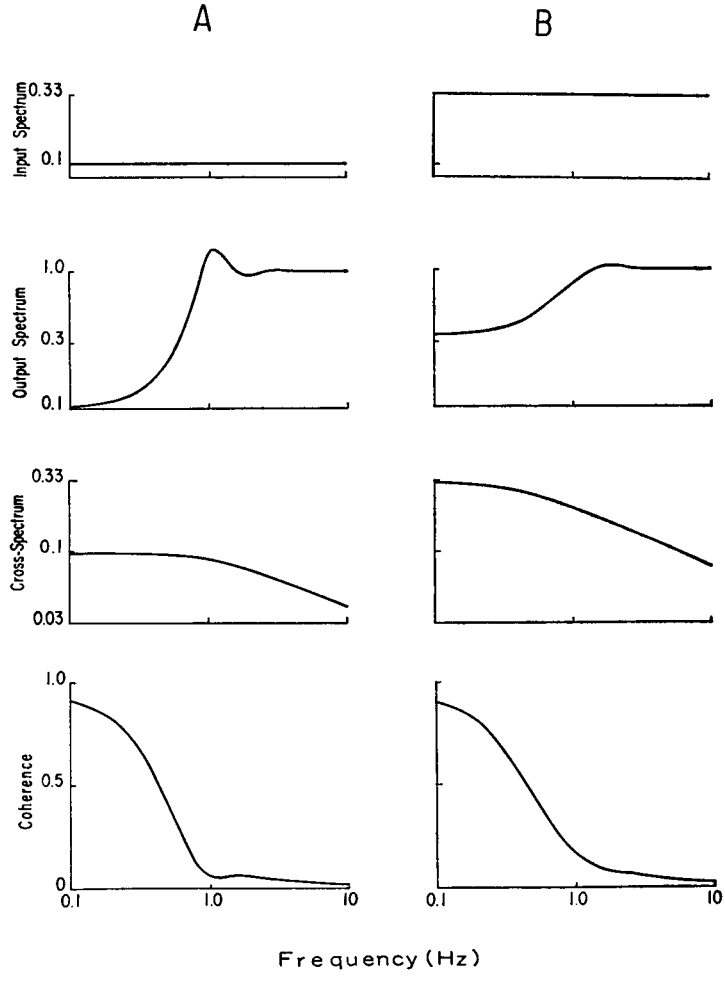

FIGURE 4 The input spectrum, output spectrum, magnitude of the cross-spectrum, and coherence function for two values of white noise applied to the perfect integrator. The mean interval (1 sec) was the same as in Fig. 3, and the noise levels were chosen in A to be $a^2 = 0.1$, and in B to be $a^2 = \frac{1}{3}$ so that the standard deviations in the interspike intervals were the same as the corresponding parts of Fig. 3. Input and output spectra were calculated from equations 3.15 and 3.17, respectively. Cross-correlation functions were calculated using equations 3.20–3.24. The cross-spectra were then obtained by computing the Fourier transforms of the cross-correlation functions according to the methods referred to in section II. Finally the coherence functions were calculated from equation 2.8.

discharge was assumed to be completely regular with a constant input. The duration of successive intervals for any real nerve cell in the absence of modulation will vary according to some probability density function $f(t)$. We can simulate this situation by using a second source of noise to model the "intrinsic" noise of the cell which is present in the absence of "extrinsic" sources. Assume both sources generate gaus-

sian white noise having spectral densities sufficient to generate root mean square fluctuations in the integrator of magnitude a_i for the intrinsic noise and a_e for the extrinsic noise. As our input to the model, we consider only the extrinsic source which will have spectral density:

$$S_x(\omega) = a_e^2/(2\pi). \tag{3.29}$$

A fraction a_e^2/a^2 of the total cross-spectrum (as given by equations 3.25 and 3.26 where $a^2 = a_e^2 + a_i^2$) will be correlated to the extrinsic source. Thus,

$$\begin{aligned} S_{xy}(\omega) &= a_e^2/(2\pi), \qquad \omega \ll c; \\ &= \frac{a_e^2}{a} \frac{c}{4\sqrt{2j\omega}}, \qquad \omega \gg c. \end{aligned} \tag{3.30}$$

The output spectrum $S_y(\omega)$ (which will depend on the total $a^2 = a_e^2 + a_i^2$) and the coherence again have simple limits. From equations 3.18, 3.19, 3.29, and 3.30:

$$\begin{aligned} \gamma^2(\omega) &= a_e^2/a_i^2, \qquad \omega \ll c; \\ &= \frac{a_e^2}{a^2} \frac{c\pi^2}{8\omega}, \qquad \omega \gg c. \end{aligned} \tag{3.31}$$

At both high and low frequencies the coherence is decreased by adding a source of noise. Effects at intermediate frequencies are also shown in Fig. 5. Because of the redistribution of the output spectrum caused by adding the intrinsic noise, the coherence is actually increased at frequencies near the carrier rate (1 Hz); however, this small increase in coherence will clearly not balance the loss of coherence at other frequencies.

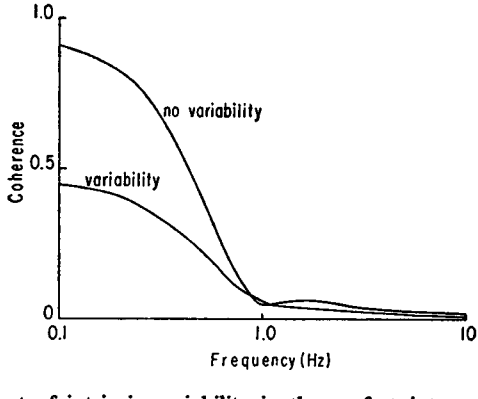

FIGURE 5 The effect of intrinsic variability in the perfect integrator on the coherence between input and output. The upper curve (no variability) is identical with that of Fig. 4 A. The lower curve was computed in a similar way, but assuming an amount of intrinsic noise equal to that applied extrinsically.

The amount of information I that the impulse train contains about the input is related to the coherence function by the following approximate equation (Stein and French, 1970):

$$I \sim -\int_0^{f_{max}} \log [1 - \gamma^2(f)] \, df, \tag{3.32}$$

where the input is limited to a frequency range $0 \leq f \leq f_{max}$. If $\log_2$ is used, the units of information are bits per second. From equation 3.31 it follows that:

$$I \sim -\int_0^{f_{max}} \log \left[1 - \frac{\pi c a_e^2}{a^2(\pi c + 16f)}\right] df.$$

This expression can be integrated and for low-frequency signals, the information transmitted is linearly related to f_{max}

$$I \backsim f_{max} \log [1 + (a_e/a_i)^2]. \tag{3.33}$$

For signals with a wide bandwidth the information transmitted only increases as the logarithm of f_{max}:

$$I \sim \frac{\pi c}{16} \frac{a_e^2}{a^2} \log f_{max}. \tag{3.34}$$

The channel capacity represents the maximum amount of information which can be transmitted under a certain constraint such as a limited bandwidth. For low-frequency signals which have a constant spectral density, a derivation similar to that of Shannon (1948) indicates that band-limited white noise will optimize the transmission of information. Thus, equation 3.33 represents an estimate of the channel capacity. This capacity can become infinite if $\gamma^2(f)$ is 1, as occurs with no intrinsic noise, and the capacity is limited by the intrinsic noise of the system. Equation 3.34 is an underestimate of the channel capacity for inputs with a wide bandwidth because advantage could be taken of the higher coherence at low frequencies. In other words, band-limited white noise would not be the optimal input, and the transmission of information could be increased by concentrating the signal power at low frequencies. Although the information transmitted by a real neuron can be estimated from equation 3.32, computation of the channel capacity will generally require knowledge of the spectral density of noise inherent in the neuron as well as an accurate model of its input-output properties.

IV. LEAKY INTEGRATOR

Sinusoidal Inputs

Now let us consider the effect on the results of section III when a nerve cell falls short of being a perfect integrator, and the responses to brief inputs decay away

exponentially with a finite time constant τ. The subthreshold voltage changes for this leaky integrator model are described by equation 1.1, and the input $x(t)$ will be assumed initially to follow equation 3.1. Substituting equation 3.1 into equation 1.1 gives the voltage as a function of the time t and the phase ϕ at $t = 0$:

$$v(t, \phi) = \frac{a\tau e^{j\phi}[e^{j\omega t} - e^{-t/\tau}]}{[1 + j\omega t]} + c\tau(1 - e^{-t/\tau}). \tag{4.1}$$

The first term on the right-hand side of equation 4.1 gives the difference in voltage Δv at any time produced by the applied sine wave, while the second term is independent of the applied sinusoid. If a voltage threshold of 1 is introduced, the time t_1 to reach threshold in the absence of sinusoidal modulation will be:

$$t_1 = -\tau \ln (1 - 1/c\tau), \tag{4.2}$$

where $c\tau > 1$ for impulses to be generated, and ln is the natural logarithm.

If an impulse is generated at a phase ϕ of a sinusoidally modulated input, the next impulse will be generated at a phase $\phi + \omega t_1$, where t_1, the time to reach threshold, is obtained by solving equation 4.1 for the first time at which the real part of $v(t_1, \phi)$ reaches 1. Methods for obtaining these values of t_1 will be described later. Similarly, if an impulse is generated at some slightly later phase $\phi + \Delta\phi$, the next impulse will occur at a phase $\phi + \Delta\phi + \omega(t_1 + \Delta t_1)$.

If over many cycles a certain number of impulses are generated in the interval between ϕ and $\phi + \Delta\phi$, the same number will be generated in the interval between $\phi + \omega t_1$ and $\phi + \Delta\phi + \omega(t_1 + \Delta t_1)$. The density of impulses $h(\phi + \omega t_1)$ at a phase $\phi + \omega t_1$, relative to that at phase ϕ, is inversely related to the sizes of these intervals, namely,

$$\frac{h(\phi + \omega t_1)}{h(\phi)} = \frac{\Delta\phi}{\Delta\phi + \omega\Delta t_1} = \left[1 + \frac{\omega\Delta t_1}{\Delta\phi}\right]^{-1}.$$

Now, with a constant threshold, one can write from the relationship between partial and total differentials

$$\Delta v = \frac{\partial v(t_1, \phi)}{\partial t_1}\Delta t_1 + \frac{\partial v(t_1, \phi)}{\partial \phi}\Delta\phi = 0,$$

so:

$$\frac{h(\phi + \omega t_1)}{h(\phi)} = \left[1 - \omega\frac{\partial v(t_1, \phi)/\partial\phi}{\partial v(t_1, \phi)/\partial t_1}\right]^{-1}, \tag{4.3}$$

where $v(t_1, \phi)$ is given by equation 4.1. Thus:

$$\frac{\partial v(t_1, \phi)}{\partial \phi} = \frac{ja\tau e^{j\phi}(e^{j\omega t_1} - e^{t_1/\tau})}{1 + j\omega t},$$

and:

$$\frac{\partial v(t_1, \phi)}{\partial t_1} = \frac{ae^{j\phi}(1 + j\omega t_1 e^{t_1/\tau} e^{j\omega t_1})}{1 + j\omega t} + ce^{-t_1/\tau}.$$

Substituting these two equations into equation 4.3 and simplifying:

$$\frac{h(\phi + \omega t_1)}{h(\phi)} = \frac{ae^{j\phi}(1 + j\omega\tau e^{t_1/\tau} e^{j\omega t_1}) + c(1 + j\omega\tau)}{(1 + j\omega\tau)(ae^{j\phi} + c)}. \tag{4.4}$$

Equation 4.4 is the basic recurrence relation for determining the density of pulses produced by a neuronal model behaving as a leaky integrator. When the time constant τ is large, and the model approaches a perfect integrator, equation 4.4 simplifies to give:

$$\frac{h(\phi + \omega t_1)}{h(\phi)} = \frac{ae^{j(\phi+\omega t_1)} + c}{ae^{j\phi} + c}. \tag{4.5}$$

Equation 4.5 will clearly hold if equation 3.3 is obeyed. Equation 3.3 will represent a necessary as well as a sufficient condition for equation 4.5 to hold, unless the applied frequency $f = \omega/2\pi$ and the carrier rate c can be expressed as an exact ratio of integers. To show this, the time scale can be transformed using inverse trigonometric functions in such a way that the voltage increases linearly in the new time scale. Impulses will then be discharged regularly at a rate ν and sinusoidal cycles will still occur regularly at a frequency f. Over time these two regular trains will go through all possible phase relationships with respect to each other, unless there is an exact ratio of integers between the two processes so that some number k impulses occur at fixed points in n sinusoidal cycles.

This represents a new proof of equation 3.3 which indicates that for a perfect integrator, the density of impulses at various phases of an applied sinusoid will be sinusoidally modulated with no change in phase and constant gain independent of frequency. To see what changes in phase and gain result in the leaky integrator, we assume initially that the same density applies to an ensemble of identical neuronal models:

$$h_0(\phi) = \nu(1 + ae^{j\phi}/c), \tag{4.6}$$

where ν, the mean frequency of each model, is chosen to satisfy the boundary condition in the absence of modulation given by equation 4.2. Then from equation 4.4, we have after one nerve impulse that the new density $h_1(\phi + \omega t_1)$, is:

$$h_1(\phi + \omega t_1) = \nu\left(1 + \frac{ae^{j(\phi+\omega t_1)}[e^{-j\omega t_1} + j\omega\tau e^{t_1/\tau}]}{c[1 + j\omega\tau]}\right). \tag{4.7}$$

Comparing equations 4.7 and 4.6 with equation 4.5, the presence of a finite time

constant has introduced an added complex ratio,

$$R = [e^{-j\omega t_1} + j\omega\tau\, e^{t_1/\tau}]/[1 + j\omega\tau],$$

into the second term of equation 4.7. The magnitude of this ratio,

$$|R| = \left(\frac{1 + (\omega\tau e^{t_1/\tau})^2 - 2\omega\tau e^{t_1/\tau} \sin(\omega t_1)}{1 + (\omega\tau)^2}\right)^{1/2}, \tag{4.8}$$

will multiply the modulation of the perfect integrator model while the phase change

$$< R = \tan^{-1}[\omega\tau e^{t_1/\tau} - \sin \omega t_1)/\cos \omega t_1] - \tan^{-1}(\omega\tau) \tag{4.9}$$

will modify that of the perfect integrator model which is always in phase with the input. The modulation ratio and the phase changes produced are plotted in Fig. 6 for two values of time constant. As τ is decreased, there is an increasing amount of gain at high frequencies, and a tendency for up to 90° phase lead at intermediate frequencies. At intermediate frequencies, peaks are also seen in the frequency response because of the presence of the sinusoidal term in equation 4.8, and so they repeat every time ωt increases by 2π or ft increases by 1. In calculating these changes, it was assumed that the modulation amplitude was small enough that the unmodulated value of t_1 could be used for equation 4.2. As the amplitude is increased further, changes will be seen because of modulation of the interval t_1.

Phase Locking

Further changes will also been seen on the second and later impulses produced by the ensemble. In fact, Rescigno et al. (1970) proved that each member of the ensemble will show a phase-locked pattern (i.e. it will discharge a finite series of impulses at particular phases of the sinusoidal input), and that this pattern repeats indefinitely. This result applies to all finite values of the time constant τ, but not to the perfect integrator ($\tau \to \infty$). If there are k impulses occurring in every n cycles, the response pattern can be specified using equation 2.1 by the series of k times, t_1, t_2, $\cdots$, t_k, or the series of k phases, ϕ_1, ϕ_2, $\cdots$, ϕ_k, at which impulses are discharged.

$$y(t) = \sum_{i=1}^{k} \delta(t - t_i) = \sum_{i=1}^{k} \delta(\phi - \phi_i). \tag{4.10}$$

Any regularly repeating response can be expanded in a Fourier series (Sokolnikoff and Redheffer, 1958).

$$y(t) = A_0/2 + \sum_{m=1}^{\infty} A_m \cos(m\omega t/n) + B_m \sin(m\omega t/n), \tag{4.11}$$

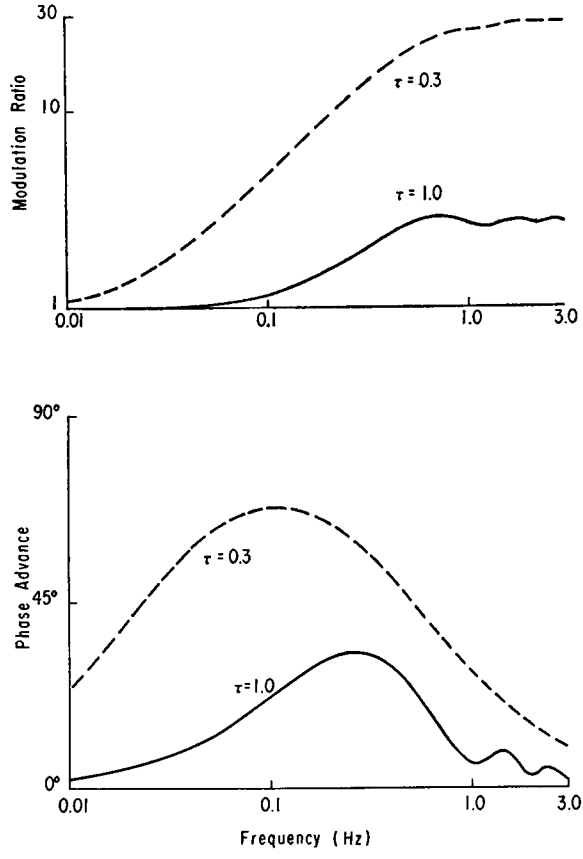

FIGURE 6 Change in modulation depth and phase after the first impulse in an ensemble of neuronal models behaving as leaky integrators. The magnitude and phase were computed for two different values of the time constant τ from equations 4.8 and 4.9 respectively. For both values of τ, the initial modulation (a/c) was assumed to be small enough to produce very small changes in the interval between impulses t_1 which was set equal to 1 sec.

where:

$$A_m = \frac{\omega}{n\pi} \int_0^{2n\pi/\omega} y(t) \cos (m\omega t/n)\, dt = \frac{\omega}{n\pi} \sum_{i=1}^{k} \cos (m\phi_i/n)$$

is the Fourier cosine coefficient,

$$B_m = \frac{\omega}{n\pi} \int_0^{2n\pi/\omega} y(t) \sin (m\omega t/n)\, dt = \frac{\omega}{n\pi} \sum_{k=1}^{k} \sin (m\phi_i/n)$$

is the Fourier sine coefficient, and ϕ_i is the phase of the ith impulse in each repetition of the pattern. The initial term in the expansion is always $k\omega/(2\pi n)$, which gives

the mean rate at which impulses are generated. For a response with $k = 1$ impulse/n cycles, the amplitude of the mth component is simply:

$$(A_m^2 + B_m^2)^{1/2} = k\omega/(n\pi),$$

and the phase of the mth component is $\tan^{-1}(-B_m/A_m) = m\phi/n$. This represents an extreme degree of modulation since the magnitude of the component at the frequency of the applied sinusoid is *twice* the mean rate of impulses. The value of ϕ can be determined from equation 4.1 setting $v(t, \phi) = 1$, and solving by a method of successive approximations.

Rescigno et al. (1970) showed that equation 4.1 can then be rewritten in the form:

$$f(\phi_i) = f(\phi_{i-1}) - e^{(\phi_{i-1}/\omega\tau)}, \tag{4.12}$$

where in our notation

$$f(\phi) = e^{(\phi/\omega\tau)}\left[1 - c\tau + \frac{a\tau e^{j\phi}}{(1 + j\omega\tau)}\right].$$

The real part of the function $f(\phi)$ will have a local maximum or minimum at phases where

$$\cos\phi = \frac{c\tau - 1}{a\tau}, \qquad \text{if } c\tau < 1 + a\tau.$$

Otherwise, the real part of $f(\phi)$ increases monotonically. In either case the maximum value in each cycle exceeds that of the previous cycle by a constant factor. Assuming an initial value ϕ_0, the cycle can be determined in which $f(\phi_1)$ first exceeds the right-hand side of equation 4.12. After finding the cycle in which the first impulse will occur, this cycle can be subdivided repeatedly, checking after each division whether $f(\phi_1)$ is less than or greater than the right-hand side of equation 4.12. ϕ_1 can then be either increased or decreased until the correct value of ϕ_1 is determined to sufficient accuracy.

If this process is repeated to determine the phases of successive impulses, the phases will begin to repeat eventually in a phase-locked pattern irrespective of the choice of ϕ_0 used to begin the computation. This phase-locked pattern can then be substituted into equation 4.11 to determine the Fourier coefficients.

The same procedure can be applied for $k = 2$ or more impulses in n cycles, and the frequency response function for phase-locked patterns containing up to 3 mpulses in n cycles are shown in Fig. 7 for two values of the time constant τ. When $\tau = 1$ prominent peaks occur whenever phase locking with $k = 1$ occurs iand smaller peaks when $k = 2$ as were seen empirically using an electronic neuronal analogue (Stein, 1970). Secondary peaks were not present in Fig. 6, so phase locking accentuates distortions which were already present in the leaky integrator model

and introduces further ones. Much larger changes in phase are also seen in Fig. 7 than in Fig. 6.

With the smaller value of the time constant ($\tau = 0.3$) in Fig. 7, the amplitudes of the responses are larger, as was true in Fig. 6, and the peaks are not as prominent; however, phase locking with $k \leq 3$ now extends over much more of the frequency range. In fact, the distortions in gain and phase now affect the transmission of sinusoids of most frequencies. The important variable in determining the extent of the phase-locked patterns with low values of k (and the corresponding distortions) is the product $\nu\tau$. If $\nu\tau \gg 1$, these patterns are not prominent. Reducing the time constant τ or the unmodulated carrier rate ν increases the effects of phase-locking. Nerve fibers which do not respond to maintained stimuli such as completely adapting mechanoreceptors (Talbot et al., 1968; Pearson and Holden, 1970) should therefore be most prone to these distortions.

The phase locking of the response also means that there will always be harmonics and, if $n > 1$, subharmonics of the modulating frequency no matter how small the input amplitude is. These distortions may be more prominent with large input amplitudes, but they will always be present when a periodic input is applied to a leaky integrator which had no intrinsic variability.

White Noise Inputs

Stimuli impinging on nerve cells will not normally be exactly periodic, but will have a certain amount of randomness. The effect of random inputs on the response to sinusoids has been discussed previously (Stein, 1970). The opposite extreme, a purely random input, has not been considered previously.

Data were obtained from an electronic neural analogue (French and Stein, 1970) adjusted to simulate the leaky integrator model with a time constant $\tau = 1$ sec and a steady rate of 1 impulse/sec in the absence of a random input. After applying white noise the best-fitting frequency response function was calculated from spectral estimates according to equation 2.7. The amplitude and phase of the frequency response function are plotted in Fig. 8 for three levels of white noise applied to the model. This figure illustrates several points:

(*a*) The peaks in the gain near 1 Hz, 2 Hz, etc., are less prominent than in the phase-locked responses (Fig. 7) and become less prominent with increasing levels of noise.

(*b*) The corresponding phase changes are also less prominent with increasing levels of noise.

(*c*) The generalized increase in gain at high frequencies seen in Fig. 6 is less prominent with white noise inputs.

(*d*) At high noise levels, the response begins to fall off for high frequencies with concomitant phase lags.

The first three effects of noise are desirable in that the distortions introduced by

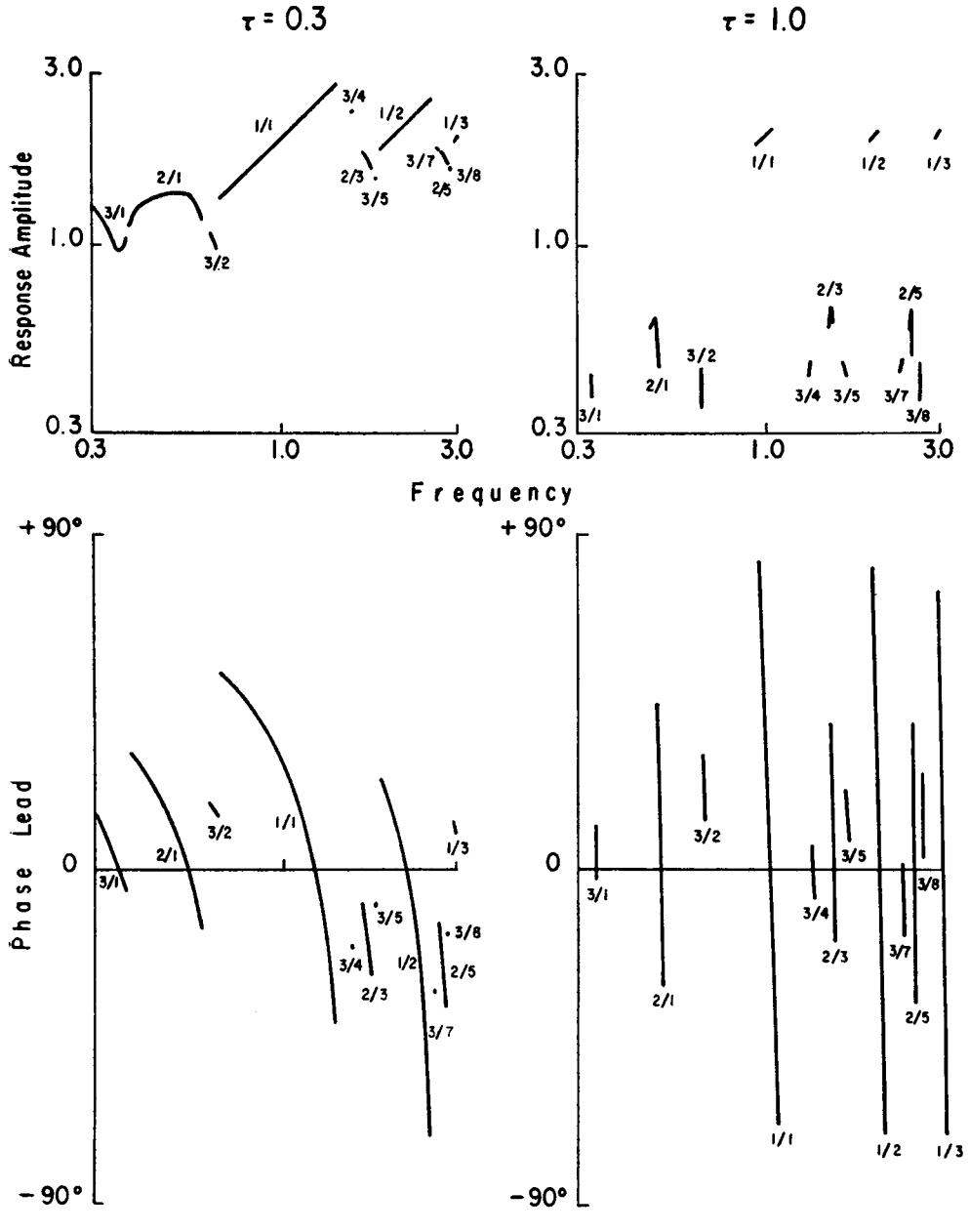

FIGURE 7 Amplitude and phase changes produced by phase-locked patterns in which k impulses are discharged by the leaky integrator for every n cycles of an applied sinusoid. The patterns are expressed as ratios (k/n) on this figure for two values of the time constant τ of the leaky integrator. For both values of τ, the mean interval was $t = 1$ sec and the ratio $a/c = 0.2$.

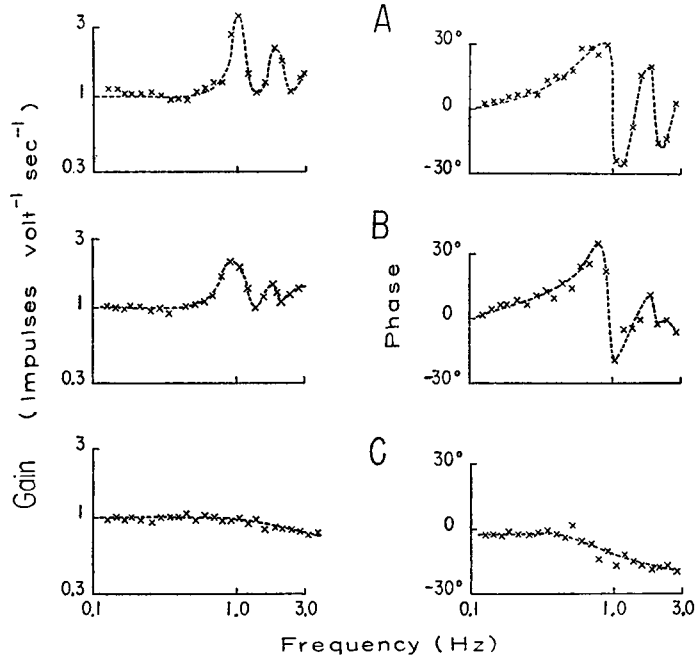

FIGURE 8 Gain and phase of the frequency response function obtained from an electronic neural analogue subjected to band-limited white noise inputs of root mean square amplitude (A) 0.19 v, (B) 0.28 v, and (C) 0.75 v. The time constant of integration was 1 sec and the carrier rate in the absence of any noise input was 1 impulse/sec.

the leaky integrator and by periodic inputs will not be apparent with suitable random input signals. The fourth effect was also seen in the perfect integrator at high noise levels (equation 3.25). These results suggest that a nerve cell whose subthreshold properties approximate those of a leaky integrator could also be used to transmit information reliably about random input signals impinging upon it. To examine this idea more carefully, we again introduce a certain amount of variability into the neuronal model to simulate the inherent variability of nerve cells.

Intrinsic Variability

Much of the discussion on the effects of intrinsic variability added to the perfect integrator can be carried over to the leaky integrator, including the derivation of equation 3.33 for the channel capacity of the model for low-frequency signals. This formula will hold over a smaller range of amplitudes and frequencies because of the greater nonlinearity of the leaky integrator and the effects discussed above which affect its high-frequency behavior. Fig. 9 shows the coherence of the discharge of the neuronal analogue with a constant intrinsic variability and increasing amounts of noise applied as an input signal. Note that the coherence is increased at

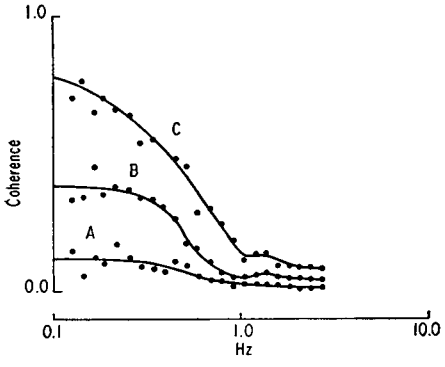

FIGURE 9

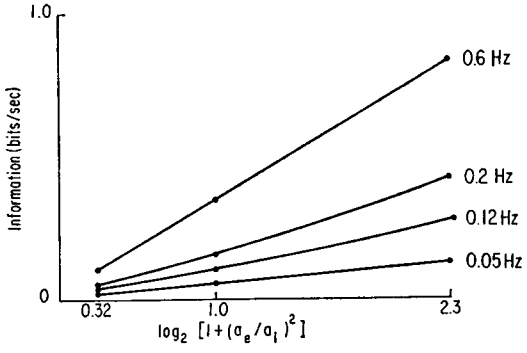

FIGURE 10

FIGURE 9 The effect of intrinsic variability in the leaky integrator on the coherence between input and output using a neuronal analogue subjected to band-limited white noise inputs. The intrinsic noise level was held constant while the coherence was evaluated for ratios of extrinsic to intrinsic power of (A) 0.25, (B) 1, and (C) 4 to 1.

FIGURE 10 Transmission of information by the leaky integrator model as a function of extrinsic, a_e, and intrinsic, a_i, input power and bandwidth. The values of the coherence function obtained in Fig. 9 were used to calculate the information transmitted using equation 3.32. For small bandwidths, the information transmitted is close to that predicted from equation 3.33.

low frequencies as expected and also that the range of frequencies having substantial values of coherence is also increased. The information capacity of the neuronal analogue as a function of bandwidth considered is shown in Fig. 10. Because of the broadened region of high coherence, the amount of information transmitted in the impulse train can increase faster than a logarithmic relation for some bandwidths.

V. DISCUSSION

In this section we will consider qualitatively the implications of the quantitative results of previous sections for coding and transmission of information by nerve cells. The first model considered, in which all subthreshold events are integrated perfectly over time, has the remarkable property (equation 3.3) of reproducing the form of a periodic input in the density of its impulses averaged over a number of cycles. Furthermore, it does this without alteration in phase and with equal gain for all frequency components. Even with a random (Poisson) process as an input, the output is completely coherent with the input at low frequencies (equation 3.13). At higher frequencies this property is lost unless there is one-to-one transmission (each impulse at the input produces an impulse at the output). The coherence at high frequencies between input and output drops to a level determined by the number of impulses at the input required to produce one impulse at the output, even though the gain at all frequencies (the magnitude of the frequency response

function) remains constant. The perfect integrator model retains its remarkable linearity for all positive-going inputs; however, if the input consists of sinusoids or white noise of sufficient amplitude that it can drive the integrator away from the threshold voltage for some time, details of this activity are not contained in the impulse train. The response is a "rectified" copy of the input, and the linear part of the response increases less rapidly with increasing levels of the input. The response also contains increasingly large components due to nonlinearities (e.g., harmonics at multiples of the applied frequencies). With white noise as an input, the variability or jitter in the intervals preferentially hinders the transmission of high-frequency signals (equation 3.25). Therefore, the frequency response function as well as the coherence declines at high frequencies (Fig. 4). The presence of a steady input, which produces a constant "carrier" rate of impulses, can counteract the tendency for rectification. Increasing the steady input broadens the range of frequencies over which the output will be strongly coherent with the input, and increases the coherence at high frequencies (equation 3.28). In contrast, adding a broad-band signal to simulate the intrinsic variability of nerve cells will decrease the coherence between other nonperiodic inputs and the output at low and at high frequencies (equation 3.31).

If there is a substantial decay of subthreshold inputs with time (leaky integrator), the gain of the model will be greater for high-frequency signals than for low-frequency ones. The gain often has maxima at frequencies near the carrier rate and multiples of carrier rate. With periodic inputs, the discharge of the model is patterned in that a sequence of impulses occurs at particular phases of the periodic signal (phase locking) and this pattern repeats indefinitely. The presence of other nonperiodic inputs to the model, or of intrinsic sources which produce a somewhat variable discharge, reduces the tendency for phase locking, and permits a more faithful replica of the input to be transmitted in the output pulse train. Even other periodic inputs may be helpful in this way (Spekreijse and Oosting, 1970); however, as with the perfect integrator, the coherence between the output and a broad-band input will be limited by the intrinsic variability of the neuronal model, particularly at low frequencies. Approximate equations (3.33–3.34) have been derived for the ability of a neuronal model or of a nerve cell to transmit information (in the sense introduced by Shannon [1948] of a number of bits per second). The methods developed permit the analysis of information transmission to be extended to time-varying signals with a broad frequency spectrum, rather than requiring constant signals which have been mainly used in the past (reviewed by Stein [1970]; see also the noteworthy early attempts to analyze time-varying signals by MacKay and McCulloch [1952] and by Rapoport and Horvath [1960]). The results indicate that more regularly discharging neurons will be more effective in transmitting information about nonperiodic signals having frequency components near or above the carrier rate, although averaging over several cycles (or several cells) may be required. Detailed consideration of these models provides a framework for under-

standing the responses of neurons which are being analyzed in this laboratory using identical methods. The methods should provide realistic estimates for the frequency response function, the coherence function, and the information capacity of nerve cells using a variety of natural inputs.

We thank Dr. E. Butz and Dr. A. Mannard for helpful comments on this manuscript.

This work was supported in part by grants from the Medical Research Council of Canada (MA-3307 and ME-3308).

Received for publication 4 June 1971.

REFERENCES

BAYLY, E. J. 1968. *I.E.E.E. (Inst. Elec. Electron. Eng.) Trans. Bio-Med. Eng.* **15**:257.

BENDAT, J. S., and A. G. PIERSOL. 1966. Measurement and Analysis of Random Data. John Wiley & Sons, Inc., New York.

CALVIN, W. H., and C. F. STEVENS. 1968. *J. Neurophysiol.* **31**:574.

COOLEY, J. W., and J. W. TUKEY. 1965. *Math. Comput.* **19**:297.

COX, D. R., and H. D. MILLER. 1965. The Theory of Stochastic Processes. Methuen and Co. Ltd., London.

DARLING, D. A., and A. J. F. SIEGERT. 1953. *Ann. Math. Statist.* **24**:624.

FRENCH, A. S., and A. V. HOLDEN. 1971 *a. Comp. Progr. Biomed.* **1**:219.

FRENCH, A. S., and A. V. HOLDEN. 1971 *b. Kybernetik.* **8**:165.

FRENCH, A. S., and R. B. STEIN. 1970. *I.E.E.E. (Inst. Elec. Electron. Eng.) Trans. Bio-Med. Eng.* **17**:248.

GERSTEIN, G. L., and B. MANDELBROT. 1964. *Biophys. J.* **4**:41.

GLUSS, B. 1967. *Bull. Math. Biophys.* **29**:233.

JOHANNESMA, P. I. M. 1968. *In* Neural Networks. E. R. Caianello, editor. Springer-Verlag KG., Berlin. 116.

JOHANNESMA, P. I. M. 1969. Stochastic neural activity—A theoretical investigation. Ph.D. Thesis. Catholic University, Nijmegen, The Netherlands.

KIANG, N.Y.-S., T. WATANABE, E. C. THOMAS, and L. F. CLARK. 1965. Discharge Patterns of Single Fibers in the Cat's Auditory Nerve. Research Monograph. No. 35. Massachusetts Institute of Technology Press, Cambridge.

KNIGHT, B. W. 1969. *In* Systems Analysis in Neurophysiology. C. Terzuolo, editor. University of Minnesota Press, Minneapolis. 61.

KNIGHT, B. W., J.-I. TOYODA, and F. A. DODGE. 1970. *J. Gen. Physiol.* **56**:421.

KNOX, C. K. 1969. *In* Systems Analysis in Neurophysiology. C. Terzuolo, editor. University of Minnesota Press, Minneapolis. 73.

LAPICQUE, L. 1907. *J. Physiol. (Paris).* **9**:622.

MACKAY, D. M., and W. S. MCCULLOCH. 1952. *Bull. Math. Biophys.* **14**:127.

MATTHEWS, P. B. C., and R. B. STEIN. 1969. *J. Physiol. (London).* **202**:59.

MCKEAN, T. A., R. E. POPPELE, N. P. ROSENTHAL, and C. A. TERZUOLO. 1970. *Kybernetik.* **6**:168.

MELVILL JONES, G., and J. H. MILSUM, 1970. *J. Physiol. (London).* **209**:295.

MOORE, G. P., D. H. PERKEL, and J. P. SEGUNDO. 1966. *Annu. Rev. Physiol.* **28**:493.

NELSEN, D. E. 1964. *Mass. Inst. Technol. Res. Lab. Electron. Quart. Tech. Rep.* **74**:168.

PARTRIDGE, L. D. 1966. *J. Theor. Biol.* **11**:257.

PEARSON, T., and A. V. HOLDEN. 1970. *Proc. Can. Fed. Biol. Soc.* **13**:38.

RAPOPORT, A., and W. J. HORVATH. 1960. *Inform. Control.* **3**:335.

RESCIGNO, A., R. B. STEIN, R. L. PURPLE, and R. E. POPPELE. 1970. *Bull. Math. Biophys.* **32**:337.

ROY, B. K., and D. R. SMITH. 1969. *Bull. Math. Biophys.* **31**:341.

SEGUNDO, J. P., D. H. PERKEL, H. WYMAN, H. HEGSTAD, and G. P. MOORE. 1968. *Kybernetik.* **4**:157.

SHANNON, C. E. 1948. The Mathematical Theory of Communication. University of Illinois Press, Urbana. Reprinted 1962.

SIEBERT, W. M. 1969. *Mass. Inst. Technol. Res. Lab. Electron. Quart. Tech. Rep.* **94**:281.
SOKOLNIKOFF, I. S., and R. M. REDHEFFER. 1958. Mathematics of Physics and Modern Engineering. McGraw-Hill Book Company, New York.
SPEKREIJSE, H., and H. OOSTING. 1970. *Kybernetik*. **7**:22.
STEIN, R. B. 1965. *Biophys. J.* **5**:173.
STEIN, R. B. 1967. *Biophys. J.* **7**:797.
STEIN, R. B. 1970. *In* The Neurosciences. Second Study Program. F. O. Schmitt, editor. The Rockefeller University Press, New York. 597.
STEIN, R. B., and A. S. FRENCH. 1970. *In* Excitatory Synaptic Mechanisms. P. Anderson and J. K. S. Jansen, editors. Oslo University Press, Oslo. 247.
SUGIYAMA, H., G. P. MOORE, and D. H. PERKEL. 1970. *Math. Biosci.* **8**:323.
TALBOT, W. H., I. DARIAN-SMITH, H. H. KORNHUBER, and V. B. MOUNTCASTLE. 1968. *J. Neurophysiol.* **31**:301.
TERZUOLO, C., editor. 1969. Systems Analysis in Neurophysiology. University of Minnesota Press, Minneapolis.